

Research Paper

Contribution of the central hydrophobic residue in the *PXP* motif of voltage-dependent K⁺ channels to S6 flexibility and gating properties

Paola Imbrici,^{1,†} Alessandro Grottesi,^{2,†} Maria Cristina D'Adamo,¹ Roberta Mannucci,⁴ Stephen J. Tucker³ and Mauro Pessia^{1,*}

¹Section of Human Physiology; Department of Internal Medicine; University of Perugia School of Medicine; Perugia, Italy; ²CASPUR; Inter-University Consortium for the Application of Super-Computing Universities and Research; Rome, Italy; ³Department of Physics; Clarendon Laboratory; University of Oxford; Oxford, United Kingdom; ⁴Section of Internal Medicine and Oncology; Department of Clinical and Experimental Medicine; University of Perugia School of Medicine; Perugia, Italy

[†]These authors contributed equally to this work.

Key words: *Shaker*, potassium channels, K_v1.1, V404, S6 helix, gating

Shaker-like (K_v1.1) channels contain a highly conserved *Pro-Val-Pro* (*PVP*) motif at the base of S6 that produces a kink in the S6 helices and provides a flexible element thought to be essential for channel gating. The role of proline-induced kinks in transmembrane helices is well known, but the contribution of the small hydrophobic valine between these two prolines is not known, and interestingly, *Shab*-like (K_v2.1) channels possess an isoleucine at this position (*PIP*). Here we show that the exact nature of this central hydrophobic residue within the *PXP* motif confers unique functional properties to K_v1 channels, including changes in activation and deactivation kinetics, voltage-dependent properties and open probabilities, but single-channel conductance and cell expression levels are not affected. In support of these functional changes, molecular dynamic simulations demonstrate that valine and isoleucine contribute differently to S6 flexibility within this motif. These results therefore indicate that the nature of the central hydrophobic residue in the *PXP* motif is an important functional determinant of K_v channel gating by contributing, at least in part, to the relative flexibility of this motif.

Introduction

Voltage-gated K⁺ channels are composed of four subunits each of which contains six transmembrane domains (TMs), S1 through S6. The S1–S4 segments comprise the voltage-sensing domain, which senses membrane potential and controls the gating of the pore domain (S5–S6). Although still controversial, it appears that upon membrane depolarization the voltage-sensing domain undergoes a movement within the membrane electric field that is mechanically transferred, via the S4–S5 linker, to the intracellular gate of the channel. The opening

of the gate at the helix-bundle crossing is thought to involve pivoted bending of the inner pore-lining helices (S6) at a highly conserved glycine residue in the middle of S6. This bending motion is then proposed to splay the TMs outwards to widen the gate and allow K⁺ to flow through the channel. Although this model has now been investigated extensively by both site-directed mutagenesis and molecular dynamics (MD) simulations, the exact movements of the S6 helices have not been entirely elucidated.^{1–5} Several lines of evidence indicates that the C-terminal portion of the S6 segment also plays an important role in K_v channel gating. A unique feature of this region of S6 is the *PVP* motif, consisting of two highly conserved prolines separated by a small hydrophobic residue. This motif is highly conserved amongst the voltage-gated K⁺ channels and is thought to act as a helix-breaking sequence inducing a bend within S6.

This *PXP* motif has also been shown to provide a flexible hinge or swivel element that regulate the gating machinery by allowing the lower half of the S6 to move.^{2,5–14} In particular, Yellen and colleagues proposed that the valine within the *PVP* motif of *Shaker* channels (V474), remains relatively stationary during channel gating and could act as a pivot point for S6 motions.¹⁴ Indeed, the crystal structure of K_v1.2, a *Shaker*-like K⁺ channel, confirmed that the *PXP* motif induces a bend that directs the S6 helix towards the S4–S5 linker, suggesting an electro-mechanical coupling between the voltage-sensing domain and the intracellular gates via the S4–S5 linker.^{15,16}

Interestingly, a sequence alignment of K_v channels reveals that K_v2.1 possesses a *PIP* motif (Fig. 1). Valine and isoleucine side chains contain two non-hydrogen moieties attached to their beta carbon, which provides a greater bulkiness near to the protein backbone, and thus a greater restriction in the conformations that the main-chain can adopt. Because of these unique properties of valine and isoleucine and their location within the *PXP* motif, we hypothesized that they influence the gating of K_v1.1 channel and the degree of S6 flexibility. We therefore used a combination of functional and computational approaches to compare the properties of human K_v1.1 channels containing either the wild-type *PVP* or mutant *PIP* motifs. Our results indicate that the precise nature of the central hydrophobic residue, and consequently the relative flexibility of the *PXP* motif contribute directly to the functional diversity of the K_v channel family.

*Correspondence to: Mauro Pessia; Associate Professor; Section of Human Physiology; Department of Internal Medicine; University of Perugia School of Medicine; Via del Giochetto; Perugia I-06126 Italy; Tel.: +39.075.5857375; Fax: +39.075.5857371; Email: pessia@unipg.it

Submitted: 10/06/08; Revised: 12/03/08; Accepted: 12/03/08

Previously published online as a *Channels* E-publication:
<http://www.landesbioscience.com/journals/channels/article/7548>

This manuscript has been published online, prior to printing. Once the issue is complete and page numbers have been assigned, the citation will change accordingly.

Results

PVP and PIP motifs confer unique biophysical properties to $K_V1.1$. Sequence alignment of the S6 segments of different K_V channels reveals that the highly conserved PVP motif of *Shaker* channels is replaced by PIP in members of the *Shab* subfamily ($K_V2.1$ and $K_V2.2$; Fig. 1). To investigate the contribution of these hydrophobic residues within the tandem proline motif, valine 404 (V-404) of the human $K_V1.1$ channel was substituted with an isoleucine (I-404). Figure 2A shows representative activating and deactivating current traces for I-404 superimposed with V-404 channels for comparison. The time constants of activation and deactivation of both channel types were determined from fitting exponential functions to the relevant currents. This revealed that the activation and deactivation rates for I-404 channels are significantly slower than V-404 (Fig. 2A). In particular, the activation $\tau_{V1/2}$ for I-404 was ~1.3-fold slower and the deactivation $\tau_{V1/2}$ ~1.6-fold slower than for wild-type V-404 channels (Table 1). This indicates that the specific nature of the residue within the PXP motif contributes directly to the kinetics of channel opening and closing.

The voltage dependence of channel activation was then investigated by recording tail currents after prepulse commands to several voltages (Fig. 2B). The Boltzmann fit to current-voltage data points showed that the midpoint activation voltage ($V_{1/2}$) for I-404 channels was shifted by ~20 mV to more positive potential with respect to V-404 (Fig. 2B, Table 1). This suggested that the open to closed state equilibrium might be affected. We therefore estimated the stability of the open state (in comparison with the closed state) by calculating the Gibbs free energy of channel opening for both channel types.¹⁷⁻¹⁹ The open-state stabilization free energy value for I-404 was ~3-fold smaller than V-404 (Table 1) suggesting that the presence of an isoleucine at this position promotes stabilization of the closed state.

To further investigate the hypothesis that this central hydrophobic residue may contribute to differences in the closed to open state equilibrium, and to investigate the role of this residue on single-channel properties, recordings of single channel activity were performed. Previous mutations within this region of S6 have shown dramatic changes in single-channel conductance, and so this parameter can be used as a test for open channel distortion.^{14,20,21}

Figure 2C shows representative current traces recorded from inside-out patches from *Xenopus* oocytes expressing V-404 and I-404 channels. The open dwell life times for both channel types were analyzed and compared. However, the time constants of the open durations for both channel types were not significantly different (Table 1) and were essentially voltage-independent in the range between 0 and +60 mV (*not shown*). Also the single-channel slope conductances were not affected (Table 1). We then calculated the open probability for both channel types, plotted them as a function of the test potentials and, fitted the data points with a Boltzmann function (Fig. 2D). The $V_{1/2}$ values, calculated from the fits, were

<i>Shaker</i>	AIAGVLTIAL PVP VIVSNFNFYFHRETDQEEMQSQNFNHVTS CPYLPG-----TLG	513
hKv1.1	AIAGVLTIAL PVP VIVSNFNFYFHRETEGEEQ--AQLLHVSS-PNLAS-----DSD	440
hKv1.2	AIAGVLTIAL PVP VIVSNFNFYFHRETEGEEQ--AQLQVTSCP KIPS-----SPD	443
hKv2.1	CIAGVLVIAL PIP IIVNNFSEFYKEQKRQEKAIKRREALERAKRNGSIVSMNMKDAFARS	453
hKv2.2	CIAGVLVIAL PIP IIVNNFSEFYKEQKRQEKAIKRREALERAKRNGSIVSMNLKDAFARS	461
hKv3.1	ALAGVLTIAM PVP VIVSNFNGMYYSLAMAKQKLPKKKKKH IPRPQLGSPNYCKSVVNSPH	480
hKv4.1	SLSGLVLVIAL PVP VIVSNFSRIYHQNRADKRRRAQQKVR LARIRLAKSGTTNAFLQYKQN	452

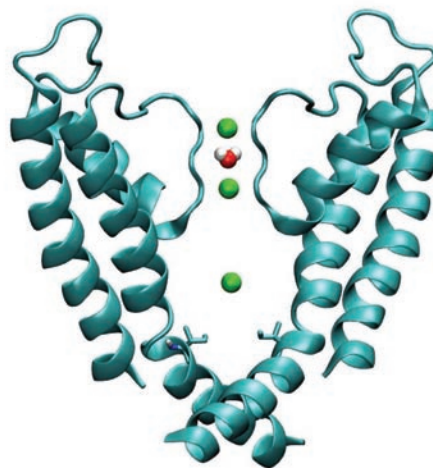


Figure 1. Sequence alignment of the S6 segment of different K_V channels. (Top) The alignment reveals that the PVP motif (**bold**), which is highly conserved in *Shaker*-like channels, is replaced by a PIP motif in *Shab*-like channels ($K_V2.1$ and $K_V2.2$). (Bottom) Schematic representation of $K_V1.1$ homology model used for MD simulations. The picture shows only two monomers side by side for clarity. The location of the I-404 residues in S6 helices of the mutated structure are highlighted as sticks. The selectivity filter in the starting configuration is also shown with K^+ ions as green spheres and a water molecule in between. The structure was then embedded in a POPC membrane bilayer and then solvated with water molecules (*not shown*).

-53.0 ± 1.4 mV ($k = 5.9 \pm 1$ mV) for V-404 channels and -38.4 ± 1.6 mV ($k = 11.4 \pm 1.9$ mV) for I-404 channels. This analysis demonstrated the open duration and the single-channel conductance were not greatly affected, but that the presence of an isoleucine in the PXP motif shifts the $V_{1/2}$ of the channel ~15 mV to more depolarized potentials and, produces a reduction in the open probability at all potentials tested (Fig. 2D). These results confirm that central residue in the PXP motif contributes to the probability of channel opening and the stability of the open state.

We also examined the C-type inactivation properties of both channel types by holding the membrane potential of oocytes at -80 mV and delivering depolarization steps to +20 mV for 3.5 min. The superimposition of these current traces did not reveal any main changes in the inactivation time course (*not shown*). Indeed, the fit of the decaying phase of the currents with exponential functions yielded time constants for V-404 and I-404 channels of 5.2 ± 1.3 s and 5.6 ± 1.1 s, respectively ($n = 10$).

We next investigated whether the valine to isoleucine substitution might cause any abnormal trafficking and/or processing of the channel to plasma membrane. We therefore analyzed the fluorescence intensity of oocytes expressing GFP-tagged variants, and measured their whole-cell current amplitudes. Our results showed that the biophysical properties of these GFP-tagged constructs were identical to the corresponding untagged channels and that both V-404 and I-404 channels generated similar whole-cell current amplitudes at +20 mV and number of channels expressed, calculated with the equation $I = N \cdot i_p$, when equal amounts of mRNA was injected

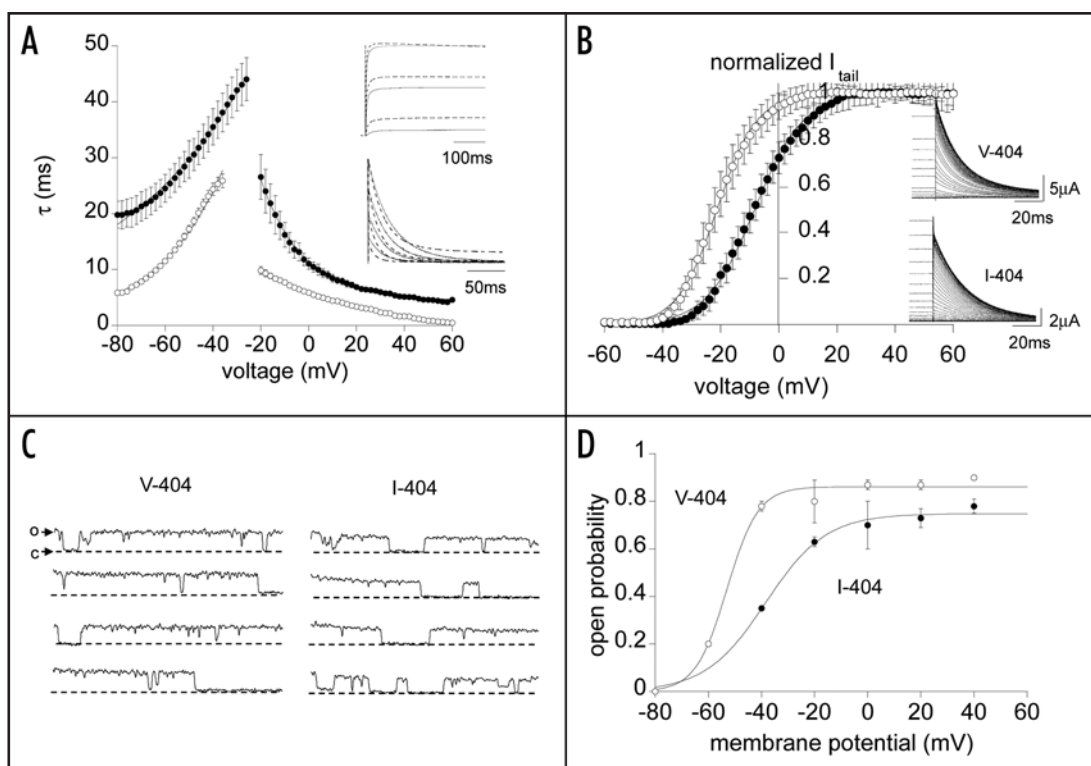


Figure 2. Biophysical properties of $K_v1.1$ channels harboring either V-404 or I-404 residue. (A) Activation and deactivation time constants as a function of voltage for V-404 (\circ) and I-404 (\bullet) channels. The data points were fitted with the equation: $\tau = \tau_{V_{1/2}} \exp[(V - V_{1/2})/k]$, where $\tau_{V_{1/2}}$ is the time constant at the mid-point activation voltage ($V_{1/2}$) of the channels, and k is the slope factor for the voltage-dependence of the time constants. Superimposed current traces (top right) for V-404 (dashed traces) and I-404 (solid traces) channels. The activating currents were evoked from a holding potential of -80 mV to +20 mV, +40 mV and +60 mV and scaled to equalize the steady-state maximal amplitude recorded at +60 mV. (Bottom right) Superimposed deactivating currents recorded at -40, -50, -60 and -70 mV after prepulse potentials to +60 mV. Currents were scaled to equalize the peak tail current amplitude recorded at -40 mV. (B) Current-voltage relationships obtained by plotting the normalized peak tail currents as a function of the pre-pulse potentials (from -60 mV to +80 mV, 3 mV increments), for V-404 (\circ) and I-404 (\bullet) channels. The solid lines represent the fit of the data points with the Boltzmann function: $NI = 1 / \{1 + \exp [(V - V_{1/2})/k]\}$ from which the $V_{1/2}$ and slope factor k were calculated (Table 1). The insets on the right hand side show representative tail currents recorded at -50 mV for the indicated channels. (C) Representative single-channel currents recorded in the inside-out configuration of the patch-clamp from oocytes expressing V-404 (left) and I-404 (right) channels. The openings were evoked by 200 ms depolarizing voltage commands to +20 mV from a holding potential of -80 mV. (D) Open probabilities as a function of test pulses for V-404 (\circ) and I-404 (\bullet) fitted with a Boltzmann function (solid lines). The data points are the mean \pm SD of 6 patches.

into oocytes (not shown). Furthermore, image analysis with confocal microscopy suggests that both constructs possess similar expression patterns and are predominantly located in the plasma membrane (Fig. 1S). These results suggest that the changes in the functional properties we observe are due to direct changes in the intrinsic biophysical properties of the channel rather than any indirect effect due to changes in processing and/or trafficking.

The central residue in the PXP motif affects the flexibility of S6. Our data so far suggest that the central residue within the PXP motif contributes directly to the function of the S6 segments of *Shaker*-like channels. Thus, to test the effects of these different PXP motifs on the mobility of the S6 we used MD simulations of the isolated S6 domain. The $K_v1.2$ channel has a PVP motif and its X-ray structure has been resolved at 2.9 Å.¹⁵ We therefore used this crystal structure to investigate the structural consequences of changes to this motif (see Methods for details). Unless otherwise stated, all analysis was carried out discarding the first 2 ns of simulation time in order to take into account the effect of the force field on the equilibrium properties of the system. Prior to further investigation, a structural check on all simulations was performed by calculating the root mean square deviation (RMSD) of the C α carbon position with respect to their

initial position as a function of time (data not shown). The average RMSD from initial positions shows that the simulation trajectories are fully consistent with a conformational drift of a folded state and the secondary structure of the V-404 and I-404 channel was retained throughout the simulations. In order to understand the effect of these hydrophobic residues on the conformational dynamics of backbone chain of the channel, we calculated the root mean square fluctuations of C α carbon atoms position of the S6 helix residues with respect to their average positions over the equilibrated portion of the MD trajectories (see Methods).

Figure 3 shows that S6 helix flexibility is higher with V-404 rather than with I-404 in the region spanning from before the putative hinge point (Gly-396 in $K_v1.1$) to beyond the 404 position (Fig. 3A and B). Not all the monomers within the channel (labeled in different colors) behave in the same way, but this is likely due to limited sampling of MD simulations.²² The C-terminus of the helix is also quite flexible, but that depends on the intrinsic flexibility of the distal termini, and these are rarely involved in hydrogen bonds or other non-bonding interactions.²³

To quantitatively address S6-helix flexibility in both wild-type and mutant channel types, we also performed a Principal Components

Table 1 **Biophysical parameters for V-404 and I-404 channels**

	V-404	I-404
Voltage-dependence of activation		
V _h (mV)	-28.1 ± 2.9	-8.6 ± 2.3**
k (mV)	7.5 ± 1.1	8.4 ± 0.7
Kinetics of activation		
τ (ms)	13.0 ± 0.2	17.4 ± 0.4**
k (mV)	34.3 ± 0.7	34.6 ± 1.6
Kinetics of deactivation		
τ (ms)	36.3 ± 0.6	57.8 ± 0.5**
k (mV)	27.8 ± 0.6	59.7 ± 0.9
C-type inactivation		
I _{final} /I _{peak}	0.16 ± 0.05	0.07 ± 0.05
τ fast (s)	5.2 ± 1.3	5.6 ± 1.1
τ slow (s)	55.4 ± 4.7	52.8 ± 6.1
Recovery from inactivation		
τ fast (s)	0.184 ± 0.03	0.242 ± 0.05
τ slow (s)	5.4 ± 0.6	7.7 ± 2.5
Free energy of channel opening at 0 mV, ΔG ₀ , (Kcal/mol)	-2.0 ± 0.6	-0.7 ± 0.3**
Open-state stabilization energy, ΔΔG ₀ (Kcal/mol)	2.2	1.3
Single-channel slope conductance (pS)	10.6 ± 0.5	10.3 ± 1.6
Mean open time at +20 mV (ms)	17.8 ± 3.7	16.4 ± 5.3

The data are the mean ± SD of 5–7 cells. **p values < 0.001, Student's t-test.

Analysis (PCA) of the positional fluctuation covariance matrix of C α atoms in the S6 helix bundle as described in Methods. PCA has proven to be useful in detecting large amplitude motions in protein dynamics by filtering out non-relevant, essentially random fluctuations from the simulation trajectories. In particular, it has been shown that the first 10 eigenvectors (e.g., the essential subspace) account for 70–80% of total protein internal motion. This approach therefore enables quantitative differences in the flexibility of proteins to be measured and can address the relative flexibility of the S6 segment in both channel types. Firstly, the eigenvalues of the fluctuation covariance matrix of the four S6 helices were plotted as a function of the eigenvector index (Fig. 4). Considering the first 10 eigenvectors only, it is evident that the first eigenvalue (which accounts for 44.4% and 28.6% of the total fluctuations in V-404 and I-404, respectively) is higher for V-404 channel than for I-404. This result is consistent with our observation that the flexibility of V-404 is higher than I-404 (Fig. 3). The second eigenvalue for I-404 channel, however, is higher than V-404, although the difference is less pronounced as it was for the first eigenvalue. Analysis of the remaining 8 eigenvalues does not suggest any remarkable difference between both channel types. Further analysis of the S6 helix flexibility was therefore restricted to the first 2 eigenvectors only. Figure 5 shows the analysis of the RMSF as filtered along the first eigenvector for V-404 and I-404 channels. Clearly, the RMSF pattern for V-404 channel, along the first principal component, is higher than I-404. In particular the region spanning from residues 392 to 410 of all V-404 S6 segments

is more mobile with respect to the flanking residues, a pattern already detected in previous simulations studies.^{5,24} The presence of an isoleucine at position 404 therefore restricts the global dynamics of the S6 helix bundle, as evidenced by a substantial reduction of these fluctuations (Fig. 5B).

Discussion

Here we show that the presence of either valine or isoleucine in the *PXP* motif of S6 confers unique gating properties and contributes to the flexibility of the S6 segment. Our functional studies demonstrate that the presence of an isoleucine within the *PXP* motif results in channels with remarkably slower opening and closing kinetics, reduced sensitivity to membrane potential depolarization and a reduced open probability compared to wild-type V-404 channels. The Gibbs free energy of channel opening and single channel properties suggest that the presence of a valine within this motif promotes a shift of the gating equilibrium towards the open state, and vice versa, isoleucine promotes a stabilization of the closed state.

Furthermore, the effects of these residues on the voltage-dependent gating of this channel are important and indicate that the *PVP* motif also probably serves an important role in the electro-mechanical coupling mechanism between the gate at the helix-bundle crossing and the voltage-sensor domain. This is supported by the fact that substitution of the equivalent valine in *Shaker* channels (V-474) with alanine, also shifts the V_{1/2} of the channel -17 mV to more negative potentials.¹³ Thus, it appears that a progressive reduction of the hydrophobicity and bulkiness of the residue between these tandem prolines produces a shift in the voltage-dependence of the channel through a range of almost 30 mV.

Our MD simulations also support this hypothesis that a *PVP* motif is more flexible than the corresponding *PIP* motif and therefore the opening motion at the helix bundle crossing might occur more easily with a valine at this hinge point than with an isoleucine.¹⁴ This is most likely due to the fact that isoleucine has a larger ethyl group attached to its C-beta carbon which would restrict the conformational flexibility of the backbone. The flexibility of S6 in K_V1.5 appears higher than that of K_V1.1, although, the biophysical properties of these channel types are similar.⁹ Sequence alignment of the S6 segments for both K_V1.1 and K_V1.5 channels reveals that they are identical, therefore, their flexibility should be comparable. A possible explanation for this apparent discrepancy could reside in the different experimental conditions, structures and simulations time: 20 ns vs. 10 ns used for our study and that of Labro et al., respectively. Likely, the conformational dynamics of the S6 domain are stabilized by the presence of S5 and P loop in the structure, resulting in smaller flexibility of the S6 compared to the same segment analyzed alone.

In conclusion, this study indicates that the nature of the central hydrophobic residue with the *PXP* motif of K_V1.1 affects channel gating by contributing to the relative flexibility of the primary gate at the helix-bundle crossing and the electro-mechanical coupling mechanism of the voltage-sensor domain.

Materials and Methods

Oocytes preparation and channel expression. Procedures involving *Xenopus laevis* and their care were conducted according to

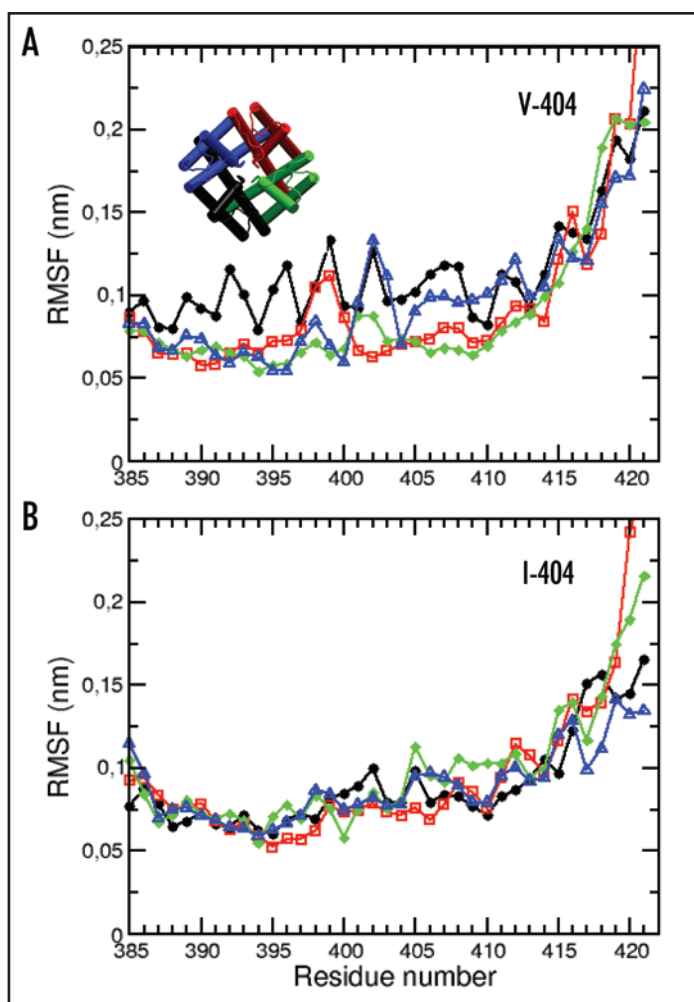


Figure 3. Molecular dynamic simulations for V-404 and I-404 channels. Root Mean Square Fluctuations (RMSF) of the $C\alpha$ carbon atoms of S6 helices as calculated from the equilibrated portion of the MD simulation for V-404 (A) and I-404 (B) channels. Residues 385–420 refer to $K_V1.1$ channels. Symbols with different colours refer to the four S6 regions from each monomer of the channel molecule and correspond to the schematic picture of the channel topology that has been drawn in the top-left corner of (A).

institutional guidelines and in compliance with national (D.L. no. 116, G.U., Suppl. 40, 18 February 1992) and international laws and policies (EEC Council Directive 86/609, OJ L 358,1, 12 December 1987; NIH Guide for the Care and Use of Laboratory Animals, NIH Publication N. 85-23, 1985 and Guidelines for the Use of Animals in Biomedical Research. The animals underwent no more than two sessions of surgery, with an interval of at least 3 weeks. *X. laevis* were anaesthetized with an aerated solution containing 3-aminobenzoic acid ethyl ester methansulphonate salt (5 mM) and sodium bicarbonate (60 mM), pH 7.3. The ovary was dissected and the oocytes digested in OR-2 solution that contained (mM): NaCl 82.5, KCl 2, $MgCl_2$ 1, HEPES 5, collagenase A 0.5 U ml^{-1} (Sigma), pH 7.50–7.55. In vitro transcribed cRNAs were microinjected into the oocytes 24 h later by using a nanoliter injector-WPI and incubated at 16°C. Typically, every oocyte was injected with 50 nl of a solution containing the relevant cRNA. The amount of cRNAs was quantified using a spectrophotometer and by ethidium bromide staining.

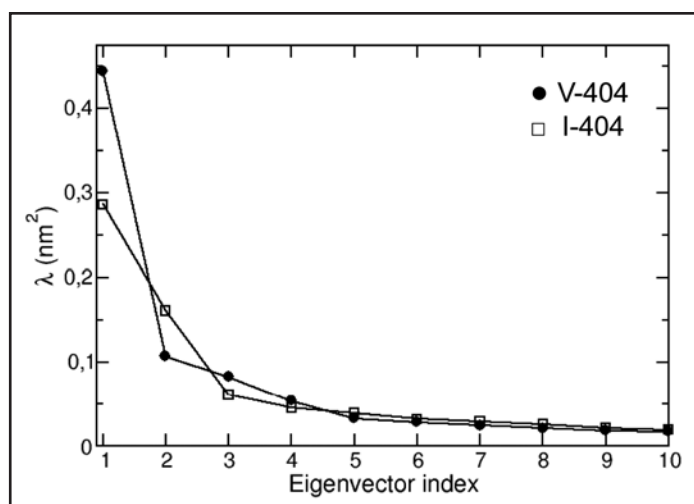


Figure 4. Eigenvalues for V-404 and I-404 channels. Eigenvalues of the positional fluctuation covariance matrix of $C\alpha$ carbon atoms of the S6 helices plotted as a function of the eigenvector index for V-404 (●) and I-404 (□). Only the first 10 eigenvectors (e.g., the essential subspace) are represented in the figure. Note that the first eigenvalue for I-404 is significantly smaller than V-404 channel.

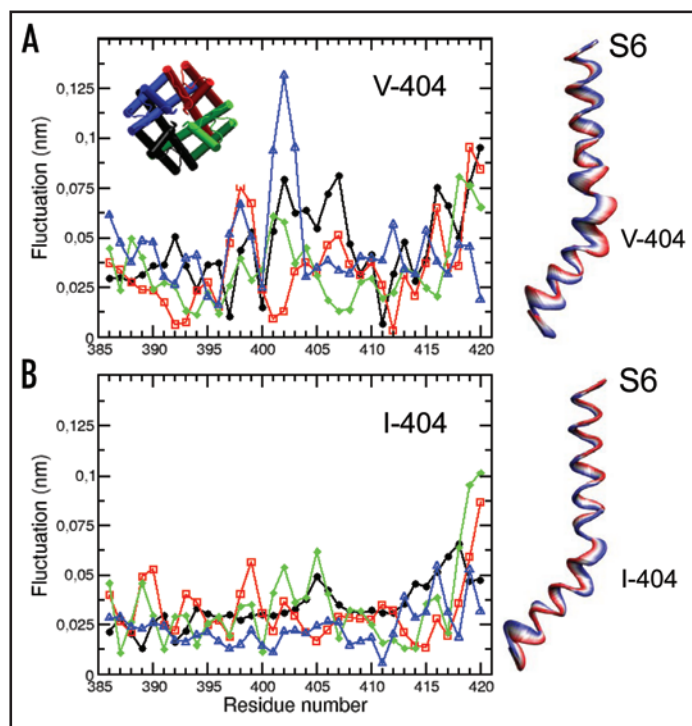


Figure 5. V-404 and I-404 confer distinct dynamic properties to S6 segments. Root Mean Square Fluctuations (RMSF) of the $C\alpha$ carbon atoms of S6 helices as calculated along the first principal component of the positional fluctuation covariance matrix for V-404 (A) and I-404 (B). A picture of $K_V1.2$ channel topology is also highlighted in the top-left corner of (A) with different colours referring to the four S6 regions and symbols of (A and B). On the right-hand side of (A and B) are shown “tube” representations of 25 snapshots of the S6 helix along the first principal component for V-404 and I-404 channels, respectively. The thickness is proportional to local helix flexibility. Channels with isoleucine residue in the PXP motif display a remarkable reduction in S6 flexibility.

Two-electrode voltage-clamp recordings. Recordings were performed from *Xenopus* oocytes at -22°C , 1–8 days after injection. A GeneClamp 500 amplifier (Axon Instruments) interfaced to a PC computer with an ITC-16 interface (Instrutech, N.Y., USA) was used. Microelectrodes were filled with 3 M KCl and had resistances of 0.1–0.5 M Ω . The recording solution contained (mM): NaCl 96, KCl 2, MgCl₂ 1, CaCl₂ 1.8, HEPES 5, pH 7.4. Currents were evoked by voltage commands from a holding potential of -80 mV as described in the figure legends. Data acquisition and analysis were performed by using: IGOR (Wavemetrics), Pulse + PulseFit (HEKA Elektronik, Germany) and KaleidaGraph (Synergy Software, USA). Leak and capacitive currents were subtracted using a P/4 protocol.

Patch-clamp recordings. Inside-out patch recordings were performed at room temperature (-22°C) by using an Axopatch 200B amplifier (Axon Instruments). The pipette solution contained (mM): NaCl 120, KCl 2, CaCl₂ 0.1, HEPES 10 (pH 7.4), whereas the cytoplasmic solution contained (mM): KCl 120, CaCl₂ 1, EGTA 11, HEPES 10, pH 7.4. Recording electrodes were pulled from 7052 glass type (Garner Glass, Calif., USA), dipped in sticky wax (Kerr, Emoryville, Calif., USA) prior to polishing, and had resistances of 3–15 M Ω . Junction potentials between bath and pipette solutions were properly nullified. The recordings were filtered at 0.5–2 kHz with a 4-pole low-pass Bessel filter and acquired at 5–10 kHz with a Pulse + PulseFit program (HEKA Elektronik, Germany). The current traces were leak subtracted by using averaged sweeps with no opening, which were fitted with exponential functions. Channel activity was analyzed with a TAC-TACfit program (Bruyton, Wash., USA) by using the 50% threshold technique to determine the duration and event amplitude. Channel openings were visually inspected before being accepted (*event-by-event* mode). Open-duration histograms were fitted with an exponential probability density function using the maximum-likelihood method. Durations were corrected for the corner frequency of the low-pass filter used when acquiring and analysing the data.²⁵ Missed events were not corrected.

Data analysis. The Gibbs free energy of channel opening at zero voltage was calculated according to Monks et al.¹⁹ as: $\Delta G_0 = zFV_{1/2}$ where z is the equivalent charge, F is the Faraday's constant and $V_{1/2}$ is the midpoint of channel activation values that were calculated from the Boltzmann fit to normalized tail currents:

$$NI = 1/\{1 + \exp[(V - V_{1/2})/k]\}$$

where k is the slope factor. The open-state stabilization free energy ($\Delta\Delta G_0$) was calculated as:

$$\Delta\Delta G_0 = \Delta G_{0\text{I-404}} - \Delta G_{0\text{V-404}}$$

Molecular biology. The V-404 and I-404 channels were generated by using the human K_v1.1 cDNA as template and the QuikChange Site-Directed Mutagenesis Kit (Stratagene) according to the manufacturer's instructions. These constructs were also tagged with GFP at the C-terminus by removing the stop codon and fusing them in frame with GFP excised from the pEGFP-C1 vector (Clontech). The nucleotide sequences of all mutant channels were determined by automated sequencing. All cDNAs were subcloned into the oocyte expression vector pBF, which provides 5' and 3' untranslated regions from the *Xenopus* β -globin gene, flanking a polylinker containing

multiple restriction sites. Capped cRNAs were synthesized in vitro, as previously described.²⁶

Confocal microscopy. Confocal microscopy of *Xenopus* oocytes, injected with GFP-tagged constructs, was performed on a Zeiss LSM 510 laser scanning confocal microscope (Jena, DE) using a 10X objective. GFP fluorescence was excited with a 488-nm argon laser beam. Emissions were collected using a 515–565-nm bandpass filter. All images were acquired with the same experimental settings (laser power, pinhole diameter and PMT gain) and Image J was used for the quantification of fluorescence emission of the pixels corresponding to the oocyte membrane. Three-dimensional reconstruction of representative images was performed with the Surpass module of Imaris software (Bitplane, Zurich, CH).

Molecular dynamics simulations. Molecular dynamics simulations were performed starting from the open pore conformation of K_v1.2. The initial protein coordinates for simulation of V-404 and the I-404 channel were taken from the Protein Data Bank (www.rcsb.org), entry code: 2A79. The simulation system consisted of a 7.50 x 9.42 x 10.19 nm box with the K_v1.2 pore domain (namely, S5-P-S6) embedded in a 170 POPC lipid bilayer and 14368 SPC water molecules. The pore domain residues were defined as extending from residue 324 to 421 of K_v1.2. All polar residues were considered in their default ionization states at pH 7.0. Initial crystal water molecules present in the structure were retained during simulations. The configuration of the selectivity filter was chosen according to Morais-Cabral et al.²⁷ Then, the system (i.e., protein plus membrane) was solvated with SPC water molecules.²⁸ Counter-ions were added where needed to keep all systems electrically neutral. The I-404 protein was generated by replacing the Val-404 side-chain with the corresponding Ile on all S6 helices of K_v1.2. After replacement, a 1000 steepest descent minimization cycle was performed on the mutated residues while keeping all other protein atoms constrained.

System set-up. For the simulations the protein was positioned in a pre-equilibrated 1-palmitoyl-2-oleoyl-phosphatidyl choline (POPC) bilayer so as to maximize all possible interaction of the POPC head-groups and the 'belts' of amphipathic aromatic side chains on the protein surface. Once the protein was inserted in the bilayer, an equilibration was performed during which the system was warmed up in a stepwise manner: 4 short time scale unrestrained MD runs (typically 50 ps) were performed at 50, 100, 200 and 250 K. Then the productive run started at 300 K for 20 ns. The initial velocities were taken randomly from a Maxwellian distribution at the desired temperature. MD simulations were performed with GROMACS 3.3.2 (www.gromacs.org) with a modified version of the GROMOS96 force field.^{29,30} Lipid parameters were based on those by Berger et al.³¹ and Marrink et al.³² The lipid-protein interactions used GROMOS parameters. Parameters derived from those of Åqvist³³ were used for the K⁺ ions. Simulations were carried out in the NPT ensemble, with periodic boundary conditions. The temperature and pressure were held constant by coupling to an external thermostat and barostat.³⁴ Long range electrostatic interactions were calculated using the Particle Mesh Ewald summation methods.³⁵ Lennard-Jones interactions were calculated using a cut-off of 0.9 nm. The pair lists were updated every ten steps. The LINCS algorithm³⁶ was used to constrain bond lengths. The timestep was 2 fs, and coordinates were saved every 0.5 ps.

Analysis. Root Mean Square Fluctuations (RMSF) of position of a selected C α carbon atoms with respect to its average position was calculated according to the following:

$$RMSF = \sqrt{\frac{1}{N} \sum_{i=1}^N (\vec{r}_i - \langle \vec{r} \rangle)^2}$$

where N is the total number of time frames used to average and \vec{r} is the element position vector at time i and $\langle \vec{r} \rangle$ is the average value.

Principal components analysis. A quantitative description of the dynamic properties of each system were analyzed by means of principal component analysis of the covariance matrix of the positional fluctuations of C α , as described elsewhere.^{37,38} Briefly, this matrix was built starting from coordinates collected on the equilibrated portion of the simulations according to the following definition:

$$C_{ij} \equiv \langle (x_i - \langle x_i \rangle)(x_j - \langle x_j \rangle) \rangle$$

where x_i and x_j run over the x , y and z coordinates of the considered atoms i and j . Diagonalization of this matrix afforded the principal directions of the large-amplitude concerted motions (e.g., the principal components or eigenvectors). Those components characterize the essential subspace of protein's internal dynamics, and describe the main directions where atomic fluctuations take place. In particular, conformational changes potentially accessible by a given principal component were calculated using the protocol described in Xu et al.³⁹ Molecular visualization and structural diagrams used VMD.⁴⁰

Acknowledgements

The financial support of Telethon-Italy (Grant GGP030159), MIUR-COFIN 2007 and COMPAGNIA di San Paolo (Turin) is gratefully acknowledged. We thank Carlo Fini for critically reading the manuscript, Ildo Nicoletti for his contribution, Domenico Bambagioni and Ezio Mezzasoma for outstanding technical assistance.

Note

Supplementary materials can be found at: www.landesbioscience.com/supplement/ImbricCHAN3-1-Sup.pdf

References

- Liu Y, Holmgren M, Jurman ME, Yellen G. Gated access to the pore of a voltage-dependent K⁺ channel. *Neuron* 1997; 19:175-84.
- del Camino D, Yellen G. Tight steric closure at the intracellular activation gate of a voltage-gated K⁺ channel. *Neuron* 2001; 32:649-56.
- Yellen G. The moving parts of voltage-gated ion channels. *Q Rev Biophys* 1998; 3:239-95.
- Bright JN, Sansom MS. K_v channel S6 helix as a molecular switch: simulation studies. *IEE Proc Nanobiotechnol* 2004; 151:17-27.
- Grottesi A, Domene C, Hall B, Sansom MS. Conformational dynamics of M2 helices in KirBac channels: Helix flexibility in relation to gating via molecular dynamics simulations. *Biochemistry* 2005; 44:14586-94.
- Tieleman DP, Shrivastava IH, Ulmschneider MR, Sansom MS. Proline-induced hinges in transmembrane helices: Possible roles in ion channel gating. *Proteins* 2001; 44:63-72.
- Bright JN, Shrivastava IH, Cordes FS, Sansom MS. Conformational dynamics of helix S6 from *Shaker* potassium channel: Simulation studies. *Biopolymers* 2002; 64:303-13.
- Labro AJ, Raes AL, Bellens I, Ottschytch N, Snyders DJ. Gating of *Shaker*-type channels requires the flexibility of S6 caused by prolines. *J Biol Chem* 2003; 278:50724-31.
- Labro AJ, Grottesi A, Sansom MS, Raes AL, Snyders DJ. A K_v channel with an altered activation gate sequence displays both "fast" and "slow" activation kinetics. *Am J Physiol Cell Physiol* 2008; 294:C1476-84.
- Sands Z, Grottesi A, Sansom MS. Voltage-gated ion channels. *Curr Biol* 2005; 15:44-7.
- Beckstein O, Biggin PC, Bond P, Bright JN, Domene C, Grottesi A, Holyoake J, Sansom MS. Ion channel gating: Insights via molecular simulations. *FEBS Lett* 2003; 555:85-90.
- del Camino D, Holmgren M, Liu Y, Yellen G. Blocker protection in the pore of a voltage-gated K⁺ channel and its structural implications. *Nature* 2000; 403:321-5.
- Hackos DH, Chang TH, Swartz KJ. Scanning the intracellular S6 activation gate in the shaker K⁺ channel. *J Gen Physiol* 2002; 119:521-32.
- Webster SM, Del Camino D, Dekker JP, Yellen G. Intracellular gate opening in *Shaker* K⁺ channels defined by high-affinity metal bridges. *Nature* 2004; 428:864-8.
- Long SB, Campbell EB, Mackinnon R. Crystal structure of a mammalian voltage-dependent *Shaker* family K⁺ channel. *Science* 2005a; 309:897-903.
- Long SB, Campbell EB, Mackinnon R. Voltage sensor of K_v1.2: Structural basis of electro-mechanical coupling. *Science* 2005b; 309:903-8.
- Hong KH, Miller C. The lipid-protein interface of a *Shaker* K⁺ channel. *J Gen Physiol* 2000; 115:51-8.
- Li-Smerin Y, Hackos DH, Swartz KJ. α -helical structural elements within the voltage-sensing domains of a K⁺ channel. *J Gen Physiol* 2000; 115:33-50.
- Monks SA, Needleman DJ, Miller C. Helical structure and packing orientation of the S2 segment in the *Shaker* K⁺ channel. *J Gen Physiol* 1999; 113:415-23.
- Ding S, Horn R. Tail end of the s6 segment: Role in permeation in shaker potassium channels. *J Gen Physiol* 2002; 120:87-97.
- Lopez GA, Jan YN, Jan LY. Evidence that the S6 segment of the *Shaker* voltage-gated K⁺ channel comprises part of the pore. *Nature* 1994; 367:179-82.
- Faraldo-Gómez JD, Forrest LR, Baaden M, Bond PJ, Carmen Domene, Patargias G, Cuthbertson J, Sansom M. Conformational sampling and dynamics of membrane proteins from 10-nanosecond computer simulations. *Proteins: Struct Func Genet* 2004; 57:779-83.
- Maity M, Lim WK, Rumbley JN, Englander SW. Protein hydrogen exchange mechanism: Local fluctuations. *Protein Sci* 2003; 12:153-60.
- Shrivastava IH, Bahar I. Common mechanism of pore opening shared by five different potassium channels. *Biophys J* 2006; 90:3929-40.
- Colquhoun D, Sigworth FJ. Fitting and statistical analysis of single-channel records. In: Sakmann B, Neher E, eds. *Single-channel recording*. 2nd Edn. New York: Plenum Press, 1995; 483-587.
- D'Adamo MC, Liu Z, Adelman JP, Maylie J, Pessia M. Episodic ataxia type-1 mutations in the hK_v1.1 cytoplasmic pore region alter the gating properties of the channel. *Embo J* 1998; 17:1200-7.
- Morais-Cabral JH, Zhou Y, MacKinnon R. Energetic optimization of ion conduction by the K⁺ selectivity filter. *Nature* 2001; 414:37-42.
- Berendsen HJC, Postma JPM, van Gunsteren WF, Hermans J. In: Pullman B, ed. *Intermolecular Forces*. Reidel: Dordrecht, 1981; 331-42.
- Lindahl E, Hess B, Van der Spoel D. GROMACS 30: A package for molecular simulation and trajectory analysis. *J Mol Model* 2001; 7:306-17.
- van Gunsteren WF, Berendsen HJC. In: *Gromos-87 Manual*. Groningen: Biomos BV, 1987.
- Berger O, Edholm O, Jahnig F. Molecular dynamics simulations of a fluid bilayer of dipalmitoylphosphatidylcholine at full hydration, constant pressure and constant temperature. *Biophys J* 1997; 72:2002-13.
- Marrink SJ, Berger O, Tieleman P, Jahnig F. Adhesion forces of lipids in a phospholipid membrane studied by molecular dynamics simulations. *Biophys J* 1998; 74:931-43.
- Åqvist J. Ion water interaction potentials derived from free-energy perturbation simulations. *J Phys Chem* 1990; 94:8021-4.
- Berendsen HJC, Postma JPM, van Gunsteren WF, Di Nola A, Haak JR. Molecular dynamics with coupling to an external bath. *J Chem Phys* 1984; 81:3684-90.
- Darden T, York D, Pedersen L. Particle mesh Ewald—an Nlog(N) method for Ewald sums in large systems. *J Chem Phys* 1993; 98:10089-92.
- Hess B, Bekker H, Berendsen HJC, Fraaije JGEM LINC: A linear constraint solver for molecular simulations. *J Comp Chem* 1997; 18:1463-72.
- Amadei A, Linssen ABM, Berendsen HJC. Essential dynamics of proteins. *Proteins: Struct Func Genet* 1993; 17:412-25.
- Garcia AE. Large-Amplitude Nonlinear Motions. *Proteins Physical Review Letters* 1992; 68:2696-9.
- Xu C, Tobi D, Bahar I. Allosteric changes in protein structure computed by a simple mechanical model: Hemoglobin T \leftrightarrow R2 transition. *J Mol Biol* 2003; 333:153-68.
- Humphrey W, Dalke A, Schulten K. VMD—visual molecular dynamics. *J Molec Graph* 1996; 14:33-8.